





RESEARCH ARTICLE | SEPTEMBER 09 2024

## A theoretical framework for robust implementation of *in situ* measurements of ocean currents and waves in dynamics of mooring systems

Special Collection: [Fluid-Structure Interaction](#)

Ulises Torres-Herrera ; Alireza Keramat ; Huan-Feng Duan (焕丰 段)  



*Physics of Fluids* 36, 096604 (2024)

<https://doi.org/10.1063/5.0221879>



### Articles You May Be Interested In

Stability analysis of moored floating offshore seamounts

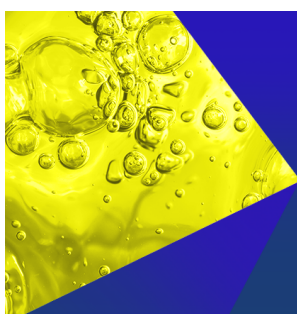
*Physics of Fluids* (November 2024)

Analysis on the split absorber integrated with taut-moored floating turbine

*Physics of Fluids* (August 2023)

Observations of sound-speed fluctuations on the New Jersey continental shelf in the summer of 2006

*J. Acoust. Soc. Am.* (February 2012)



**Physics of Fluids**  
Special Topics  
Open for Submissions

[Learn More](#)

# A theoretical framework for robust implementation of *in situ* measurements of ocean currents and waves in dynamics of mooring systems

Cite as: Phys. Fluids **36**, 096604 (2024); doi: [10.1063/5.0221879](https://doi.org/10.1063/5.0221879)

Submitted: 4 June 2024 · Accepted: 18 August 2024 ·

Published Online: 9 September 2024



Ulises Torres-Herrera, Alireza Keramat, and Huan-Feng Duan (煥丰 段)

## AFFILIATIONS

Department of Civil and Environmental Engineering, The Hong Kong Polytechnic University, Hong Kong 999077, People's Republic of China

**Note:** This paper is part of the special topic, Fluids-Structure Interaction.

<sup>a)</sup>Author to whom correspondence should be addressed: [hf.duan@polyu.edu.hk](mailto:hf.duan@polyu.edu.hk)

## ABSTRACT

We develop an approximated method to solve analytically the equations of motion that describe mooring line dynamics in a one-dimensional model. For the first time, we derive integral closed-form expressions to compute dynamic properties of mooring lines subject to ocean currents and waves of arbitrary time and spatial dependence, in terms of modified Bessel functions. This is done by decomposing the mooring line in three regions where different approximations and mathematical techniques of solution are carried out. Our analytical results provide a robust framework to simulate and analyze extreme realistic oceanic events when data from *in situ* ocean observation systems are available, regardless of the resolution or coarseness of subsurface measurements and even for long acquisition times. In order to prove the advantages of this approach, we have processed data from two stations in the National Data Buoy Center of the National Oceanic and Atmospheric Administration. From simulations with ocean currents data, we have gained insights into the coupling of the spatial modulation of ocean currents with the characteristic wavelengths of elastic lines. From simulations with ocean waves data, we have defined a scheme to analyze wave data and identify the contribution of each subset of frequency peaks to the net fluctuation of mooring line tension. This could be useful for classification of irregular waves based on their impact on mooring line tension. The development of better tools that integrate theoretical and experimental findings is necessary for the assessment of marine structures under the environmental conditions associated with climate change.

Published under an exclusive license by AIP Publishing. <https://doi.org/10.1063/5.0221879>

## I. INTRODUCTION

Mooring lines are a very important element of many oceanic installations across the ocean and coastal areas. Despite being one of the oldest and simplest devices for providing stability and safety to offshore facilities, it is still the most extended method nowadays. This is justified by their low cost and by the flexibility and manageability of their installation (Ma *et al.*, 2019; Ruzzo *et al.*, 2021; and Ja'e *et al.*, 2022).

Despite all the achievements of mooring lines in floating structures, one of the main disadvantages in their operation is related to their instability under critical environmental conditions, leading to line breakages that may put in risk the safety of an entire oceanic platform or facility (Du *et al.*, 2020; Cheng *et al.*, 2021), with high economical

and even environmental costs (Sinsabvarodom *et al.*, 2021), for instance, when structural instability occurs in petroleum platforms (Yang *et al.*, 2021).

The dynamic properties of mooring lines have been studied in the literature by computational and experimental means. Theoretical studies are focused on the prediction of conditions that lead to mechanical instability and high tension regions within a mooring line (de Lange *et al.*, 2007; Governo *et al.*, 2023). Such computations allow them to carry out several simulations varying key design parameters and environmental conditions on the mooring system; this strategy provides guidelines for an improved design of mooring lines, avoiding conditions of difficult operation in real offshore floating structures (Tang *et al.*, 2022).

Along with all the progress achieved, these studies have intrinsic limitations. First, computational studies rely on complex, computationally expensive simulations, which limit each parametric study to a very narrow range of each variable of interest (Hong and Shah, 2018; Desiré *et al.*, 2023). In particular, the numerical simulation of mooring lines affected by currents and waves is achievable by coupling of elastic beam models with computational fluid dynamics simulations (Ghafari and Dardel, 2018; Governo *et al.*, 2023). Such simulations require very high resolution in time discretization for convergence, making it difficult to accurately incorporate realistic currents/winds/waves interaction. The accurate simulation of the intricate frequency spectrum of irregular waves, encompassing multiple frequency bands spread along a wide range of values, is very challenging for any computational tool (Matha *et al.*, 2011; Fu *et al.*, 2019; and Subbulakshmi *et al.*, 2022).

In this direction, experimental models and studies have shed light on a better description and characterization of realistic currents and waves (Barrera *et al.*, 2019; Tang *et al.*, 2022). This experimental measurements provide useful data that can be used to complement theoretical studies and, in many cases, to validate approximated theoretical models (Azcona *et al.*, 2017; Shun-Han Yang *et al.*, 2020). Still, the scaling laws that allow for an extrapolation from in-lab studies to realistic ocean-scale mooring systems are a current challenge.

The aforementioned challenges are even more important when simulations or experiments of mooring lines seek to incorporate realistic *in situ* ocean measurements. First, because the realistic conditions are difficult to reproduce or extrapolate from experimental measurements, given the limited size of laboratory equipment and facilities (Aranha and Pinto, 2001; Kuehl and Sheremet, 2014). Second, because realistic ocean data involve many time and spatial scales, which increase computational cost and challenge numerical stability and validity of simulations. These limitations are particularly relevant to study anomalous ocean events, which is the current challenge to be solved in the design and adaptation of oceanic infrastructure to face climate change (Grare *et al.*, 2013; Janssen and Janssen, 2019; and Shrira and Almelah, 2020).

In the context of complex dynamical systems, analytical methods emerge as an alternative because they can offer qualitative physical insights and computations for a much lower cost and without numerical limitations and artifacts, inherent to even the most sophisticated numerical methods for complex dynamic systems, based mostly on Finite-Element Methods. Analytical methods have been used scarcely, mostly to find simplified expressions that are developed for limit asymptotic conditions related to time-scales separation or related to small deformations; nonetheless, these expressions are very useful to validate and verify newly developed models or numerical schemes of solution, since even the most sophisticated model must accomplish certain limit cases and bounds. In such regard, analytical solutions allow for a robust validation of models (Zurigat *et al.*, 2010; Ramadan *et al.*, 2017; and Torres-Herrera and Corvera Poiré, 2021).

Typical assumptions employed to find analytical solutions of complex dynamic systems rely on the separation between two scales, namely, fast and slow dynamic variables, in such a way that external environmental conditions drive the mooring line affecting one time-scale more than the other (Bernitsas and Garza-Rios, 1998; Aranha and Pinto, 2001; and Hong and Shah, 2018). However, it has been demonstrated that such assumptions are not accomplished for mooring lines under some extreme or challenging conditions, such as in

deep waters (Ali *et al.*, 2020). A general framework is necessary to study mooring lines dynamics by analytical techniques that can be used in a wide range of physical conditions, which do not rely on the separation of time or spatial scales and do not lead to spurious anomalous results when employed under extreme conditions. Such a robust framework allows for the implementation of realistic ocean dynamics measurements and conditions with confidence.

In this work, we propose an approximated method to solve analytically the equations of motion, namely, the vibration equations as typically called in the context of structural engineering, which describe mooring line dynamics. We have employed a linearized model that still conveys the main physical features of mooring line dynamics, since it has been previously validated against three-dimensional numerical computations and also against experimental data (Aranha and Pinto, 2001). The presented analytical results are used to incorporate ocean current and wave dynamics taken from two stations in the National Data Bouy System, which are located very close to one another and allow us to get complementary information. Finally, we test and discuss the capabilities and potential of our theoretical framework for analysis of complex ocean events.

## II. MODEL

This work departs from the linearized model developed by Aranha and Pinto (2001). In this model, it is studied an elastic line subject to a viscous drag force caused by the surrounding ocean currents, where torsional and flexural rigidity effects are neglected; then, it is assumed that the deformation field depends only on one spatial coordinate, namely, the axial coordinate. With these assumptions, the model considers that the mooring line dynamics can be computed as a sum of two contributions: first, a static contribution given by the classical catenary equations in the absence of ocean waves and currents; second, a dynamic contribution that describes the deviation of transversal displacement, longitudinal displacement, local tension, and angle of the mooring line, measured with respect to the static configuration. Afterward, small deformation considerations allow one to compute the dynamic properties as linear partial differential equations with spatial-dependent coefficients given in terms of parameters associated with the static configuration. In such a way, the dynamic contribution of mooring line displacements, tension, and angle are affected by the static configuration and by the presence of ocean currents and an oscillation exerted at the top of the mooring line by ocean waves. The system is depicted in Fig. 1, and further mathematical details involved in the derivation of the model are found in Triantafyllou (1982) and Aranha *et al.* (1993).

### A. Governing equations

The model is given by the following set of equations for the dynamic variables, namely, the dynamic longitudinal displacement  $u(s, t)$ , dynamic transversal displacement  $v(s, t)$ , dynamic tension  $T_D(s, t)$ , and dynamic angle  $\varphi(s, t)$  (Aranha and Pinto, 2001),

$$m \frac{\partial^2 u}{\partial t^2} = \frac{\partial T_D}{\partial s} - T \frac{d\theta}{ds} \varphi, \quad (1)$$

$$(m + m_a) \frac{\partial^2 v}{\partial t^2} = -k_d \left( \frac{\partial v}{\partial t} - V_c(s, t) \right) + \frac{d\theta}{ds} T_D + T \frac{\partial \varphi}{\partial s} + \varphi \frac{dT}{ds}, \quad (2)$$

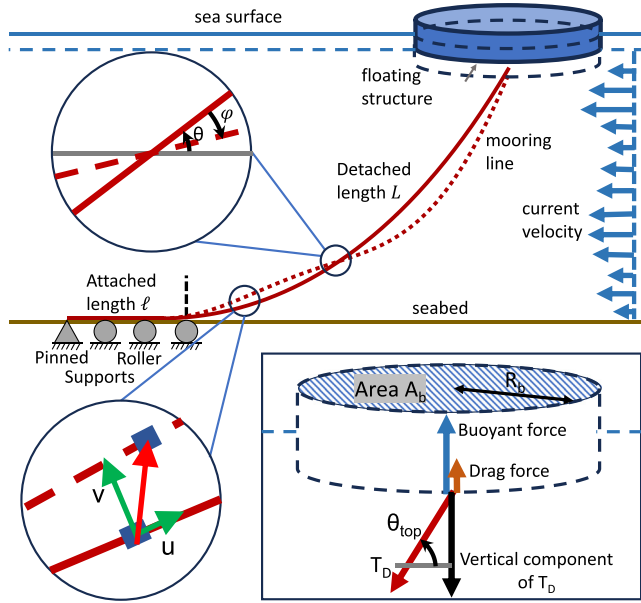


**FIG. 1.** Description of the system. The mooring line consists of an elastic tube that moves departing from a static catenary configuration, described by the transversal displacement  $v(s, t)$  and the axial displacement,  $u(s, t)$  around equilibrium position. The mooring line is surrounded by an oceanic current, characterized by a time- and space-dependent flow velocity profile  $V_c(s, t)$ .

$$T_D = EA \left( \frac{\partial u}{\partial s} - \frac{d\theta}{ds} v \right), \quad (3)$$

$$\varphi = \frac{\partial v}{\partial s} + \frac{d\theta}{ds} u, \quad (4)$$

where  $s$  is the axial coordinate along the deformed mooring line,  $t$  is the time,  $m$  is the mooring line mass per unit length,  $m_a$  is the added mass per unit length,  $k_d$  is the drag coefficient,  $V_c(s, t)$  is the current velocity field of ocean current acting on the mooring line,  $\theta(s)$  is the angle formed between the local tangent of mooring line and the horizontal axes at the initial equilibrium configuration, whereas its derivative  $\frac{d\theta}{ds}(s)$  corresponds to the local curvature of the mooring line at static equilibrium configuration,  $T(s)$  is the local tension at the equilibrium configuration. Finally,  $E$  is the elastic Young's modulus of the material that constitutes the mooring line and  $A$  is the cross-sectional area of the mooring line.

Then, we rewrite Eqs. (1)–(4) in terms of dimensionless parameters

$$\begin{aligned} \tilde{t} &\equiv \omega_c t, \quad \tilde{s} \equiv \frac{s}{L}, \quad \tilde{T} \equiv \frac{T}{EA}, \quad \tilde{m} \equiv \frac{m}{m + m_a}, \quad \tilde{k} \equiv \frac{k_d L}{\sqrt{EA(m + m_a)}}, \\ \tilde{u} &\equiv \frac{u}{L}, \quad \tilde{v} \equiv \frac{v}{L}, \quad \tilde{T}_D \equiv \frac{T_D}{EA}, \quad \tilde{V}_c \equiv \frac{V_c}{\omega_c L}, \quad \omega_c \equiv \frac{1}{L} \sqrt{\frac{EA}{m + m_a}}, \end{aligned} \quad (5)$$

where  $L$  stands for length of the portion of mooring line that is detached from the seabed. With this adimensionalization, the following set of equations is obtained:

$$\tilde{m} \frac{\partial^2 \tilde{u}}{\partial \tilde{t}^2} = \frac{\partial \tilde{T}_D}{\partial \tilde{s}} - \tilde{T} \frac{d\theta}{ds} \varphi, \quad (6)$$

$$\frac{\partial^2 \tilde{v}}{\partial \tilde{t}^2} = -\tilde{k} \left( \frac{\partial \tilde{v}}{\partial \tilde{t}} - \tilde{V}_c(\tilde{s}, \tilde{t}) \right) + \frac{d\theta}{ds} \tilde{T}_D + \tilde{T} \frac{\partial \varphi}{\partial \tilde{s}} + \varphi \frac{d\tilde{T}}{ds}, \quad (7)$$

$$\tilde{T}_D = \frac{\partial \tilde{u}}{\partial \tilde{s}} - \frac{d\theta}{ds} \tilde{v}, \quad (8)$$

$$\varphi = \frac{\partial \tilde{v}}{\partial \tilde{s}} + \frac{d\theta}{ds} \tilde{u}. \quad (9)$$

From Eqs. (6)–(9), a useful approach is to perform Fourier transform in time in order to obtain the following expressions:

$$-\tilde{\omega}^2 \tilde{m} \hat{u} = \frac{d\hat{T}_D}{d\tilde{s}} - \tilde{T} \frac{d\theta}{ds} \hat{\varphi}, \quad (10)$$

$$-\tilde{\omega}^2 \hat{v} = -\tilde{k} (-i\tilde{\omega} \hat{v} - \hat{V}_c(\tilde{s}, \tilde{\omega})) + \frac{d\theta}{ds} \hat{T}_D + \tilde{T} \frac{d\hat{\varphi}}{d\tilde{s}} + \hat{\varphi} \frac{d\tilde{T}}{ds}, \quad (11)$$

$$\hat{T}_D = \frac{d\hat{u}}{d\tilde{s}} - \frac{d\theta}{ds} \hat{v}, \quad (12)$$

$$\hat{\varphi} = \frac{d\hat{v}}{d\tilde{s}} + \frac{d\theta}{ds} \hat{u}, \quad (13)$$

where  $\hat{u}(\tilde{s}, \tilde{\omega})$ ,  $\hat{v}(\tilde{s}, \tilde{\omega})$ ,  $\hat{T}_D(\tilde{s}, \tilde{\omega})$ , and  $\hat{\varphi}(\tilde{s}, \tilde{\omega})$  denote the Fourier transform of their respective dimensionless quantities in time domain (A double superscript notation, for instance,  $\hat{\tilde{u}}$ , is omitted here for simplicity of notation).

As a consequence of the linearization, this model overlooks details about the tension field along the radial coordinate of the mooring line, and it only focuses on the local changes along the axial one. However, this level of detail is still sufficient to get an adequate picture of the dynamic motion and tension of the mooring line. Nonetheless, this model has been proved successfully with experimental data, showing a considerable range, where its results match well with the ones of complex simulations with ORCAFlex and even a wider range in which the qualitative trend between ORCAFlex and this model is still followed, while the relative error reaches values around 10–20% (Aranha and Pinto, 2001).

## B. Boundary conditions and incorporation of ocean wave dynamics

Boundary conditions for the bottom part of mooring line account for the portion of line that is attached to the seabed by pinned and roller supports. In consequence, there are points where axial and transversal displacements vanish, as follows:

$$\hat{u} \left( \tilde{s} = -\frac{l}{L} \right) = 0, \quad (14)$$

$$\hat{v}(\tilde{s} = 0) = 0. \quad (15)$$

The aforementioned boundary conditions correspond completely with the ones employed by Aranha and Pinto (2001). However, our boundary conditions for the top part of mooring line differ significantly from theirs. In the work done by Aranha and Pinto (2001), they considered that the top part of mooring line was moving in a single-frequency mode of amplitude and phase already imposed by an external actuator. However, in this work, we have extended the model to consider explicitly the role of dynamics of ocean waves acting on the

floating structure. Our results allow us to compute the actual amplitude and phase of the floating structure motion in response to an arbitrary time-dependent wave.

The boundary conditions at the attachment point of the mooring line and the floating structure are given by the force balance between the buoyant force and the mooring tension. In particular, buoyant force is caused by changes in the water level affected by the waves, whereas changes in mooring tension at the attachment point are given by the dynamic term of tension,  $T_D$  (see lower right panel of Fig. 1). For consistency between the floating structure considerations and the model of mooring line, the dynamics of the floating structure departs from an equilibrium position and considers moderate vertical displacement of the floating structure, such as the submersed region has a constant cross-sectional area or with a small dependence on vertical coordinate. Since we are considering a flat floating structure with high base-to-height ratio, we can assume neglect of the influence of air currents and precession motion (Huguet *et al.*, 2020). In such a way, we only need to account for the measured data of changes in local sea level as a function of time in order to compute accurately the buoyant forces. In these conditions, the force balance of the floating structure affected by waves is presented as follows:

$$m_b \frac{d^2 y_b}{dt^2} = -(\rho_b - \rho_w) A_b g (y_w(t) - y_b(t)) - K_{db} \left( \frac{dy_b}{dt} - \frac{dy_w}{dt} \right) - T_D(s = L, t) \sin \theta_{top}, \quad (16)$$

where  $y_w(t)$  stands for the sea level measured with respect to the equilibrium position of the structure,  $y_b$  stands for the position of the floating structure measured with respect to its equilibrium point, and  $K_{db}$  stands for the drag coefficient of the floating structure in water. In addition,  $m_b$  is the floating structure mass,  $\rho_w$  and  $\rho_b$  are water and platform density, respectively,  $A_b$  is the platform base area, and  $g$  is the gravity constant. Finally,  $\theta_{top}$  corresponds to the angle of mooring line evaluated at the attachment point, namely,  $s = L$ , at any time. In principle, such angle is computed as  $\theta_{top} = \theta(s = L) + \varphi(s = L, t)$ . However, in the model employed for mooring line dynamics, it is assumed that the dynamic angle  $\varphi(s, t)$  is smaller than the static angle  $\theta(s)$ , so we approximate  $\theta_{top} \approx \theta(s = L)$  in this work.

Then, we consider that the vertical motion of floating structure is equal to the displacement of mooring line at the attachment point, as

$$u(s = L, t) = y_b(t) \sin \theta_{top}, \quad (17)$$

$$v(s = L, t) = y_b(t) \cos \theta_{top}, \quad (18)$$

and substitution of force balance in Eq. (16) into the equality of floating and mooring displacement in Eqs. (17) and (18), leads to the following expressions for the boundary conditions in Fourier domain and in dimensionless variables:

$$\hat{u}(\tilde{s} = 1, \tilde{\omega}) = \hat{y}_w(\tilde{\omega}) Q \sin \theta_{top} + \frac{EA}{L} \sin^2 \theta_{top} \times \left( \frac{d\hat{u}}{d\tilde{s}}(\tilde{s} = 1, \tilde{\omega}) - \frac{d\theta}{d\tilde{s}}(\tilde{s} = 1) \hat{v}(\tilde{s} = 1, \tilde{\omega}) \right), \quad (19)$$

$$\hat{v}(\tilde{s} = 1, \tilde{\omega}) = \hat{y}_w(\tilde{\omega}) Q \cos \theta_{top} + \frac{EA}{L} \sin \theta_{top} \cos \theta_{top} \times \left( \frac{d\hat{u}}{d\tilde{s}}(\tilde{s} = 1, \tilde{\omega}) - \frac{d\theta}{d\tilde{s}}(\tilde{s} = 1) \hat{v}(\tilde{s} = 1, \tilde{\omega}) \right), \quad (20)$$

where  $\hat{y}_w$  is the Fourier transform in time of dimensionless water sea level  $\tilde{y}_w$ , defined as

$$\tilde{y}_w \equiv \frac{y_w}{L}, \quad (21)$$

while parameters  $K_b$  and  $Q$  are defined as

$$K_b \equiv (\rho_w - \rho_b) A_b g, \quad Q \equiv \frac{-K_b + i\tilde{\omega} \omega_c K_{db}}{-K_b + i\tilde{\omega} \omega_c K_{db} + \tilde{\omega}^2 \omega_c^2 m_b}, \quad (22)$$

where  $\hat{y}_w(\tilde{\omega})$  stands for the Fourier transform in time of the dynamic level of sea water.

### III. ANALYTICAL SOLUTION

In order to solve Eqs. (10)–(13) by analytical means, we consider that mooring line is split into three regions, where different physical approximations and considerations can be done. This is an important requirement to achieve an analytical solution in each region; then by considerations of continuity in the displacement and deformation fields of the mooring line, the solution of all the regions is coupled. It is important to point out that the definition of such regions allows us to obtain a complete solution for the mooring dynamics, which is both accurate and physically consistent for all ranges of values of the physical parameters. To the best of our knowledge, such a comprehensive and robust treatment has not been developed for the modeling and simulation of mooring systems. The details of such procedure are explained as follows. The three regions necessary to solve mooring line dynamics are mathematically defined as

$$\tilde{u}(\tilde{s}, \tilde{t}) = \begin{cases} \tilde{u}_I(\tilde{s}, \tilde{t}) & \text{if } -\frac{l}{L} \leq \tilde{s} < 0, \\ \tilde{u}_{II}(\tilde{s}, \tilde{t}) & \text{if } 0 \leq \tilde{s} < s_{th}, \\ \tilde{u}_{III}(\tilde{s}, \tilde{t}) & \text{if } s_{th} \leq \tilde{s} \leq 1, \end{cases} \quad (23)$$

$$\tilde{v}(\tilde{s}, \tilde{t}) = \begin{cases} \tilde{v}_I(\tilde{s}, \tilde{t}) & \text{if } -\frac{l}{L} \leq \tilde{s} < 0, \\ \tilde{v}_{II}(\tilde{s}, \tilde{t}) & \text{if } 0 \leq \tilde{s} < s_{th}, \\ \tilde{v}_{III}(\tilde{s}, \tilde{t}) & \text{if } s_{th} \leq \tilde{s} \leq 1, \end{cases} \quad (24)$$

where  $s_{th}$  denotes the transition value between regions II and III. A clear understanding of its physical meaning and the difference between regions II and III will be provided in Sec. III C, while its importance for the accuracy of the analytical solution will be detailed in Sec. IV. Equivalent expressions to Eqs. (23) and (24) can be defined in Fourier domain; they are omitted here for the sake of economy in space.

#### A. Solution for the first region

The first region is the portion of mooring line, of length  $l$ , that is attached to the seabed in such a way that it cannot develop transversal motion but only longitudinal stretching. Under these conditions, ocean flow velocity goes parallel to the mooring line so  $V_c = 0$ , while the terms  $\tilde{T}(\tilde{s})$  and  $\frac{d\theta}{d\tilde{s}}(\tilde{s})$  are given by the following expressions:



$$\tilde{T}(\tilde{s}) = \frac{H}{EA}, \quad \text{for } -\frac{l}{L} \leq \tilde{s} \leq 0, \quad (25)$$

$$\frac{d\theta}{d\tilde{s}}(\tilde{s}) = 0, \quad \text{for } -\frac{l}{L} \leq \tilde{s} \leq 0, \quad (26)$$

where  $H$  denotes the horizontal component of static tension, which is independent of coordinate  $\tilde{s}$ . Then, the equations of motion (6)–(9) for the region I, in terms of the variables  $u \rightarrow u_I$ ,  $v \rightarrow v_I$ ,  $\hat{T}_D \rightarrow \hat{T}_{D,I}$ , and  $\hat{\phi} \rightarrow \hat{\phi}_I$ , are given as follows:

$$-\tilde{\omega}^2 \tilde{m} \hat{u}_I = \frac{d\hat{T}_{D,I}}{d\tilde{s}}, \quad (27)$$

$$\hat{v}_I = 0, \quad (28)$$

$$\hat{T}_{D,I} = \frac{d\hat{u}_I}{d\tilde{s}}, \quad (29)$$

$$\hat{\phi}_I = 0. \quad (30)$$

In order to find the solution for  $u_I(\tilde{s}, \tilde{\omega})$ , Eqs. (27) and (29) can be combined in a single equation as

$$\frac{d^2 \hat{u}_I}{d\tilde{s}^2} + \tilde{m} \tilde{\omega}^2 \hat{u}_I = 0. \quad (31)$$

Equation (31) is a linear homogeneous second-order differential equation, whose solution is given by

$$\hat{u}_I(\tilde{s}, \tilde{\omega}) = B_1 \cos(\tilde{s} \tilde{\omega} \sqrt{\tilde{m}}) + B_2 \sin(\tilde{s} \tilde{\omega} \sqrt{\tilde{m}}), \quad (32)$$

where  $B_1$  and  $B_2$  denote the coefficients to be computed when accounting for boundary conditions, which will be detailed later.

## B. Solution for the second region

For the second and third regions, the static parameters  $\frac{d\theta}{d\tilde{s}}(\tilde{s})$  and  $\tilde{T}(\tilde{s})$  are computed departing from the catenary differential equation, as presented in Irvine and Caughey (1974), as follows:

$$\tilde{T}(\tilde{s}) = \frac{H}{EA} \sqrt{1 + \left( \frac{mgL\tilde{s}}{H} \right)^2}, \quad \text{for } 0 \leq \tilde{s} \leq 1, \quad (33)$$

$$\frac{d\theta}{d\tilde{s}}(\tilde{s}) = \frac{mgL}{H} \left( \frac{1}{1 + \left( \frac{mgL\tilde{s}}{H} \right)^2} \right), \quad \text{for } 0 \leq \tilde{s} \leq 1. \quad (34)$$

The second region is the detached portion of mooring line that is close to the seabed. For this region, we consider that the spatial variation of static parameters  $\tilde{T}(\tilde{s})$  and  $\frac{d\theta}{d\tilde{s}}(\tilde{s})$  is negligible in comparison with the spatial derivatives of mooring displacement. This is justified by analyzing the behavior of  $\tilde{T}(\tilde{s})$  and  $\frac{d\theta}{d\tilde{s}}(\tilde{s})$  in Eqs. (33) and (34) for small values of  $\tilde{s}$ . In simple terms, this means that we approximate static tension and curvature of mooring line as a first-order Taylor expansion around  $\tilde{s} = 0$  in Eqs. (33) and (34). Since both  $\tilde{T}(\tilde{s})$  and  $\frac{d\theta}{d\tilde{s}}(\tilde{s})$  are even functions of  $\tilde{s}$ , first-order coefficient vanishes, leading to

$$\tilde{T}(\tilde{s}) \approx \frac{H}{EA} + \mathcal{O}(\tilde{s}^2), \quad \text{for } 0 \leq \tilde{s} \leq s_{th}, \quad (35)$$

$$\frac{d\theta}{d\tilde{s}}(\tilde{s}) \approx \frac{mgL}{H} + \mathcal{O}(\tilde{s}^2), \quad \text{for } 0 \leq \tilde{s} \leq s_{th}. \quad (36)$$

In consequence, when expressions of  $\tilde{T}(\tilde{s})$  and  $\frac{d\theta}{d\tilde{s}}(\tilde{s})$  in Eqs. (48) and (35) are substituted into Eqs. (10)–(13), the following simplification is obtained:

$$-\tilde{\omega}^2 \tilde{m} \hat{u}_{II} = \frac{d\hat{T}_{D,II}}{d\tilde{s}} - \varepsilon \gamma \hat{\phi}_{II}, \quad (37)$$

$$-\tilde{\omega}^2 \hat{v}_{II} = -\tilde{k}(-i\tilde{\omega} \hat{v}_{II} - \hat{V}_c(\tilde{s}, \tilde{\omega})) + \gamma \hat{T}_{D,II} + \varepsilon \frac{d\hat{\phi}_{II}}{d\tilde{s}}, \quad (38)$$

$$\hat{T}_{D,II} = \frac{d\hat{u}_{II}}{d\tilde{s}} - \gamma \hat{v}_{II}, \quad (39)$$

$$\hat{\phi}_{II} = \frac{d\hat{v}_{II}}{d\tilde{s}} + \gamma \hat{u}_{II}, \quad (40)$$

where the constant parameters  $\gamma \equiv \frac{mgL}{H}$  and  $\varepsilon \equiv \frac{H}{EA}$  are defined. Equations (37)–(40) are a system of coupled linear non-homogeneous first-order differential equations, whose solution is carried by decoupling the equations using the formalism of differential operators. First step is to rewrite such equations in a matrix form, as follows:

$$\frac{d}{d\tilde{s}} \begin{pmatrix} u_{II} \\ u_{II} \\ T_{D,II} \\ \phi_{II} \end{pmatrix} = \begin{pmatrix} 0 & \gamma & 1 & 0 \\ -\gamma & 0 & 0 & 1 \\ -\tilde{m}\tilde{\omega}^2 & 0 & 0 & \varepsilon\gamma \\ 0 & -\frac{\tilde{\omega}}{\varepsilon}(\tilde{\omega} + i\tilde{k}) & -\frac{\gamma}{\varepsilon} & 0 \end{pmatrix} \begin{pmatrix} u_{II} \\ u_{II} \\ T_{D,II} \\ \phi_{II} \end{pmatrix} + \begin{pmatrix} 0 \\ 0 \\ 0 \\ -\frac{\tilde{k}}{\varepsilon} \hat{V}_c(\tilde{s}, \tilde{\omega}) \end{pmatrix}. \quad (41)$$

Eigenvalues of Eq. (41) are given in terms of the roots of the determinant equation  $\det(\underline{M} - \lambda \underline{I}) = 0$ , where  $\underline{M}$  denotes the characteristic matrix associated with Eq. (41). Computation of the determinant equation is presented as follows:

$$\varepsilon \lambda^4 + (2\varepsilon\gamma^2 + i\tilde{k}\tilde{\omega} + \tilde{\omega}^2(1 + \tilde{m}\varepsilon))\lambda^2 + (\gamma^2 - \tilde{\omega}(i\tilde{k} + \tilde{\omega}))(\varepsilon\gamma^2 - \tilde{m}\tilde{\omega}^2) = 0. \quad (42)$$

Thus, the roots of the characteristic polynomial in Eq. (42), i.e., the eigenvalues, are of the form

$$\lambda_1 = i\sqrt{a+b} \quad \lambda_2 = -i\sqrt{a+b} \quad \lambda_3 = i\sqrt{a-b} \quad \lambda_4 = -i\sqrt{a-b}. \quad (43)$$

Afterward, the corresponding eigenvectors are computed, in order to obtain the homogeneous solution for variables  $\hat{u}_{II}$ ,  $\hat{v}_{II}$ ,  $\hat{T}_{D,II}$ , and  $\hat{\phi}_{II}$  as a linear combination of terms of the form  $e^{\lambda_j \tilde{s}}$ . Finally, the method of variation of parameters is carried out to compute the independent term of the solution. The complete solution for  $\hat{u}(\tilde{s}, \tilde{\omega})$  and  $\hat{v}(\tilde{s}, \tilde{\omega})$  is presented as follows:

$$\begin{aligned} \hat{u}_{II}(\tilde{s}, \tilde{\omega}) &= \frac{(1+\varepsilon)\gamma\sqrt{a+b}}{-(a+b) + \tilde{m}\tilde{\omega}^2 + \varepsilon\gamma^2} (C_1 \cos(\tilde{s}\sqrt{a+b}) - C_2 \sin(\tilde{s}\sqrt{a+b})) \\ &+ \frac{(1+\varepsilon)\gamma\sqrt{a-b}}{-(a-b) + \tilde{m}\tilde{\omega}^2 + \varepsilon\gamma^2} (C_3 \cos(\tilde{s}\sqrt{a-b}) - C_4 \sin(\tilde{s}\sqrt{a-b})) \\ &+ \frac{\tilde{k}\gamma(1+\varepsilon)}{2b\varepsilon} \int_0^{\tilde{s}} \hat{V}_c(\tilde{s}', \tilde{\omega}) \left( \cos((\tilde{s}-\tilde{s}')\sqrt{a+b}) - \cos((\tilde{s}-\tilde{s}')\sqrt{a-b}) \right) d\tilde{s}', \end{aligned} \quad (44)$$

$$\begin{aligned} \hat{v}_{II}(\tilde{s}, \tilde{\omega}) = & C_1 \cos(\tilde{s}\sqrt{a+b}) + C_2 \sin(\tilde{s}\sqrt{a+b}) \\ & + C_3 \cos(\tilde{s}\sqrt{a-b}) + C_4 \sin(\tilde{s}\sqrt{a-b}) \\ & + \frac{\tilde{k}}{2b\varepsilon} \left( \frac{-\gamma^2\varepsilon + \tilde{m}\tilde{\omega}^2 - (a+b)}{\sqrt{a+b}} \right) \\ & \times \int_0^{\tilde{s}} \tilde{V}_c(\tilde{s}', \tilde{\omega}) \sin((\tilde{s} - \tilde{s}')\sqrt{a+b}) d\tilde{s}' \\ & - \frac{-\gamma^2\varepsilon + \tilde{m}\tilde{\omega}^2 - (a-b)}{\sqrt{a-b}} \\ & \times \int_0^{\tilde{s}} \tilde{V}_c(\tilde{s}', \tilde{\omega}) \sin((\tilde{s} - \tilde{s}')\sqrt{a-b}) d\tilde{s}', \quad (45) \end{aligned}$$

where the coefficients  $C_1$ ,  $C_2$ ,  $C_3$ , and  $C_4$  are constants to be computed accounting for the boundary conditions. Such conditions will be detailed later, along with the conditions for the constants  $B_1$  and  $B_2$  encountered previously for the solution of region I.

### C. Solution for the third region

The third region is the portion of mooring line where the static tension has reached a linear dependence on axial coordinate, so the approximation as a constant parameter no longer holds. In those conditions, the first step is to substitute  $\varphi$  and  $\tilde{T}_D$  from Eqs. (12) and (13) into Eqs. (10) and (11), leading to the following expressions:

$$\begin{aligned} \frac{d^2\hat{u}}{d\tilde{s}^2} + \left( \tilde{m}\tilde{\omega}^2 - \tilde{T} \left( \frac{d\theta}{d\tilde{s}} \right)^2 \right) \hat{u} - (1 + \tilde{T}) \frac{d\theta}{d\tilde{s}} \frac{d\hat{v}}{d\tilde{s}} - \frac{d^2\theta}{d\tilde{s}^2} \hat{v} = 0, \quad (46) \\ (1 + \tilde{T}) \frac{d\theta}{d\tilde{s}} \frac{d\hat{u}}{d\tilde{s}} + \left( \tilde{T} \frac{d^2\theta}{d\tilde{s}^2} + \frac{d\tilde{T}}{d\tilde{s}} \frac{d\theta}{d\tilde{s}} \right) \hat{u} + \tilde{T} \frac{d^2\hat{v}}{d\tilde{s}^2} + \frac{d\tilde{T}}{d\tilde{s}} \frac{d\hat{v}}{d\tilde{s}} \\ + \left( \tilde{\omega}^2 + i\tilde{\omega}\tilde{k} - \left( \frac{d\theta}{d\tilde{s}} \right)^2 \right) \hat{v} = -\tilde{k}\tilde{V}_c(\tilde{s}, \tilde{\omega}). \quad (47) \end{aligned}$$

Equations (46) and (47) were obtained without loss of generality and still apply both to regions II and III. From this point, in region III, the value of coordinate  $\tilde{s}$  is smaller but close to unit, and the parameter  $\gamma \equiv \frac{mgL}{H}$  is much larger than unit. With these considerations, it is possible to consider both  $\gamma \gg 1$  and  $\gamma\tilde{s} \gg 1$ . This is helpful to approximate curvature  $\frac{d\theta}{d\tilde{s}}(\tilde{s})$  in Eq. (34) and static tension  $\tilde{T}(\tilde{s})$  in Eq. (33), along with their first derivative, as follows:

$$\frac{d\theta}{d\tilde{s}}(\tilde{s}) = \frac{\gamma}{1 + \gamma^2\tilde{s}^2} \approx \frac{1}{\gamma\tilde{s}^2} \quad \text{for } \gamma\tilde{s} \gg 1, \quad (48)$$

$$\frac{d^2\theta}{d\tilde{s}^2}(\tilde{s}) = -\frac{2\gamma^3\tilde{s}}{(1 + \gamma^2\tilde{s}^2)^2} \approx -\frac{2}{\gamma\tilde{s}^3} \quad \text{for } \gamma\tilde{s} \gg 1, \quad (49)$$

$$\tilde{T}(\tilde{s}) = \varepsilon\sqrt{1 + \gamma^2\tilde{s}^2} \approx \varepsilon\gamma\tilde{s} \quad \text{for } \gamma\tilde{s} \gg 1, \quad (50)$$

$$\frac{d\tilde{T}}{d\tilde{s}}(\tilde{s}) = \frac{\varepsilon\gamma^2\tilde{s}}{\sqrt{1 + \gamma^2\tilde{s}^2}} \approx \varepsilon\gamma \quad \text{for } \gamma\tilde{s} \gg 1. \quad (51)$$

It is important to point out that the approximation carried out in Eqs. (48)–(51) leads to a divergence in  $\tilde{s} = 0$ . This situation is not a problem in our theoretical framework, since the proposed solution in three regions involves another approximation in the surroundings of  $\tilde{s} = 0$  (already presented in Sec. III B). Hence, the existence of region

II guarantees the absence of any divergence and requires to state the condition  $s_{th} > 0$  in order to achieve mathematical and physical consistency in the proposed analytical solution.

Substitution of the approximated coefficients  $\tilde{T}$ ,  $\frac{d\tilde{T}}{d\tilde{s}}$ ,  $\frac{d\theta}{d\tilde{s}}$ , and  $\frac{d^2\theta}{d\tilde{s}^2}$  shown in Eqs. (48)–(51) into Eqs. (46) and (47) leads to the following result:

$$\frac{d^2\hat{u}}{d\tilde{s}^2} + \left( \tilde{m}\tilde{\omega}^2 - \frac{\varepsilon}{\gamma\tilde{s}^3} \right) \hat{u} - \left( \frac{1}{\gamma\tilde{s}^2} + \frac{\varepsilon}{\tilde{s}} \right) \frac{d\hat{v}}{d\tilde{s}} + \frac{2}{\gamma\tilde{s}^3} \hat{v} = 0, \quad (52)$$

$$\begin{aligned} \left( \frac{1}{\gamma\tilde{s}^2} + \frac{\varepsilon}{\tilde{s}} \right) \frac{d\hat{u}}{d\tilde{s}} - \frac{\varepsilon}{\tilde{s}^2} \hat{u} + \varepsilon\gamma\tilde{s} \frac{d^2\hat{v}}{d\tilde{s}^2} + \varepsilon\gamma \frac{d\hat{v}}{d\tilde{s}} + \left( \tilde{\omega}^2 + i\tilde{\omega}\tilde{k} - \frac{1}{\gamma^2\tilde{s}^4} \right) \hat{v} \\ = -\tilde{k}\tilde{V}_c(\tilde{s}, \tilde{\omega}). \quad (53) \end{aligned}$$

Finally, since we are working under the assumption of large values of  $\gamma$ , it is possible to consider as well that the terms proportional to  $\frac{1}{\gamma}$  are negligible in comparison with the ones proportional to  $\gamma^0$ , and at the same time, the terms proportional to  $\gamma^0$  are negligible in comparison with the ones proportional to  $\gamma^1$ . With this assumption, we are taking the leading terms, i.e., the terms with highest-order powers of  $\gamma$  in Eqs. (52) and (53), and the following set of equations is obtained:

$$\frac{d^2\hat{u}_{III}}{d\tilde{s}^2} + \tilde{m}\tilde{\omega}^2\hat{u}_{III} - \frac{\varepsilon}{\tilde{s}} \frac{d\hat{v}_{III}}{d\tilde{s}} = 0, \quad (54)$$

$$\varepsilon\gamma\tilde{s} \frac{d^2\hat{v}_{III}}{d\tilde{s}^2} + \varepsilon\gamma \frac{d\hat{v}_{III}}{d\tilde{s}} + (\tilde{\omega}^2 + i\tilde{\omega}\tilde{k})\hat{v}_{III} = -\tilde{k}\tilde{V}_c(\tilde{s}, \tilde{\omega}). \quad (55)$$

It is noticeable that Eq. (55) only depends on  $\hat{v}_{III}$  and not on  $\hat{u}_{III}$ , so it can be solved first. This equation is a non-homogeneous second-order differential equation with variable coefficients. In order to compute the analytical solution for the homogeneous differential equation associated with Eq. (55), the following change of variable is defined:

$$x \equiv \sqrt{-\frac{4\tilde{s}}{\varepsilon\gamma}} (\tilde{\omega}^2 + i\tilde{\omega}\tilde{k}), \quad (56)$$

which transforms the homogeneous equation associated with Eq. (55) into the following expression:

$$x^2 \frac{d^2\hat{v}_{III}}{dx^2} + x \frac{d\hat{v}_{III}}{dx} - x^2\hat{v}_{III} = 0. \quad (57)$$

Equation (57) corresponds to the modified Bessel differential equation for the case of order  $n = 0$ . Thus, the homogeneous part is given in terms of the zeroth order modified Bessel functions of the first and second kind, denoted by  $I_0(x)$  and  $K_0(x)$ , respectively. Subsequently, the solution of the non-homogeneous part is carried out by variation of parameters. The complete solution for  $\hat{v}_{III}(\tilde{s}, \tilde{\omega})$  is presented as follows:

$$\begin{aligned} \hat{v}_{III}(\tilde{s}, \tilde{\omega}) = & E_1 I_0(\sqrt{\alpha\tilde{s}}) + E_2 K_0(\sqrt{\alpha\tilde{s}}) + \frac{2\tilde{k}}{\varepsilon\gamma} \int_{s_{th}}^{\tilde{s}} \sin((\tilde{s} - \tilde{s}')\tilde{\omega}\sqrt{\tilde{m}}) \\ & \times \int_{s_{th}}^{\tilde{s}'} \tilde{V}_c(\tilde{s}'', \tilde{\omega}) \left( I_1(\sqrt{\alpha\tilde{s}'} K_0(\sqrt{\alpha\tilde{s}''}) + K_1(\sqrt{\alpha\tilde{s}'} I_0(\sqrt{\alpha\tilde{s}''})) \right) d\tilde{s}'' d\tilde{s}', \quad (58) \end{aligned}$$

where  $\alpha \equiv -\frac{4}{\varepsilon\gamma} (\tilde{\omega}^2 + i\tilde{\omega}\tilde{k})$ . To the best of our knowledge, this is the first time that the role of modified Bessel functions is explored in the dynamics of mooring systems.

Then, the solution for  $\hat{v}_{III}$  is substituted from Eq. (58) into Eq. (54). After such substitution, the equation can be solved as a non-homogeneous second-order linear differential equation for  $\hat{u}_{III}$ , as follows:

$$\begin{aligned} \hat{u}_{III}(\tilde{s}, \tilde{\omega}) = & \frac{\varepsilon}{2\tilde{\omega}\sqrt{\tilde{m}}} \int_{s_{th}}^{\tilde{s}} \sqrt{\frac{\alpha}{(\tilde{s}')^3}} \sin\left((\tilde{s} - \tilde{s}')\tilde{\omega}\sqrt{\tilde{m}}\right) \\ & \times (E_1 I_1 \sqrt{\alpha\tilde{s}'} - E_2 K_1 \sqrt{\alpha\tilde{s}'} ) d\tilde{s}' + E_3 \sin(\tilde{s}\tilde{\omega}\sqrt{\tilde{m}}) \\ & + E_4 \cos(\tilde{s}\tilde{\omega}\sqrt{\tilde{m}}) - \frac{\tilde{k}}{\tilde{\omega}\gamma\sqrt{\tilde{m}}} \int_{s_{th}}^{\tilde{s}} \sqrt{\frac{\alpha}{(\tilde{s}')^3}} \sin\left((\tilde{s} - \tilde{s}')\tilde{\omega}\sqrt{\tilde{m}}\right) \\ & \times \int_{s_{th}}^{\tilde{s}'} \hat{V}_c(\tilde{s}'', \tilde{\omega}) \left( I_1 \sqrt{\alpha\tilde{s}'} K_0 \sqrt{\alpha\tilde{s}''} + K_1 \sqrt{\alpha\tilde{s}'} I_0 \sqrt{\alpha\tilde{s}''} \right) d\tilde{s}'' d\tilde{s}', \end{aligned} \quad (59)$$

where the constants  $E_1$ ,  $E_2$ ,  $E_3$ , and  $E_4$  are to be computed when boundary conditions are solved, along with the constants  $B_1$ ,  $B_2$ ,  $C_1$ ,  $C_2$ ,  $C_3$ , and  $C_4$ , that were obtained during the solution of regions I and II.

For the solution of all the aforementioned coefficients, it is necessary to include boundary conditions of continuity of displacement and tension fields in the transition point between regions I and II, denoted by  $\tilde{s} = 0$ , and the transition point between regions II and III, denoted by  $\tilde{s} = s_{th}$ . Such conditions are presented as follows:

$$\hat{u}_I(\tilde{s} = 0, \tilde{\omega}) = \hat{u}_{II}(\tilde{s} = 0, \tilde{\omega}), \quad (60)$$

$$\frac{d\hat{u}_I}{d\tilde{s}}(\tilde{s} = 0, \tilde{\omega}) = \frac{d\hat{u}_{II}}{d\tilde{s}}(\tilde{s} = 0, \tilde{\omega}), \quad (61)$$

$$\hat{u}_{II}(\tilde{s} = s_{th}, \tilde{\omega}) = \hat{u}_{III}(\tilde{s} = s_{th}, \tilde{\omega}), \quad (62)$$

$$\frac{d\hat{u}_{II}}{d\tilde{s}}(\tilde{s} = s_{th}, \tilde{\omega}) = \frac{d\hat{u}_{III}}{d\tilde{s}}(\tilde{s} = s_{th}, \tilde{\omega}), \quad (63)$$

$$\hat{v}_{II}(\tilde{s} = s_{th}, \tilde{\omega}) = \hat{v}_{III}(\tilde{s} = s_{th}, \tilde{\omega}), \quad (64)$$

$$\frac{d\hat{v}_{II}}{d\tilde{s}}(\tilde{s} = s_{th}, \tilde{\omega}) = \frac{d\hat{v}_{III}}{d\tilde{s}}(\tilde{s} = s_{th}, \tilde{\omega}). \quad (65)$$

The following step is to construct the system of algebraic equations for the coefficients by substituting the general solutions for  $\hat{u}_I$ ,  $\hat{u}_{II}$ ,  $\hat{v}_{II}$ ,  $\hat{v}_{III}$ , and  $\hat{u}_{III}$  encountered in Eqs. (32), (44), (45), (59), and (58) into the boundary conditions in Eqs. (14), (15), (19), (20), and (60)–(65). The coefficients  $B_1$ ,  $B_2$ ,  $C_1$ ,  $C_2$ ,  $C_3$ ,  $C_4$ ,  $E_1$ ,  $E_2$ ,  $E_3$ , and  $E_4$  are given by the solution of the  $10 \times 10$  system of algebraic equations just described, which is a straightforward procedure that we omit in this work for the sake of economy in space. A summary of the whole procedure to incorporate the different data in the analytical solution is shown in Fig. 2.

#### IV. VALIDATION

The analytical solution developed in Sec. III has been constructed to be used in all range of physical parameters. The separation of regions was done in order to apply different considerations in each region and then put them together in order to obtain an expression that works for all cases, approximately. In consequence, the next step is the validation and appropriate choice of the parameter  $s_{th}$  that leads to a good agreement between the analytical approximation and an accurate numerical solution of the model. It is important to notice that the analytical method required a positive-defined parameter  $s_{th}$ , which delimits region II and region III within our theoretical treatment. By

construction, the approximations carried out to achieve an analytical solution are only related to assumptions on the value of  $\gamma$  for a system. Therefore, it is expected that the free parameter  $s_{th}$  is only a function of  $\gamma$ . This means that the choice of a specific value of the parameter  $s_{th}$  is done by looking for the best agreement between the analytical and numerical results. In general, it is possible to carry out a fit for each value of the parameter  $\gamma$ , in order to find the best value of  $s_{th}$ ; in consequence, the optimal  $s_{th}$  will be slightly different for each value of  $\gamma$ . By trial and error, we have found that the optimal values follow approximately a general trend, i.e., that such values are close to  $s_{th} = 1$  for  $\gamma \leq 4$  (which implies removing region III in these conditions), while  $s_{th} = 1/\gamma$  for  $\gamma > 4$ .

Analytical results are validated against a numerical solution computed via Wolfram Mathematica utilities. For validation, we study the dynamics in case where there is a mono-modal wave of the form  $\frac{y_w(t)}{L} = U_w e^{i\omega t}$  and no ocean current, i.e.,  $V_c(s, t) = 0$ . Then, we can compute the dynamic response of the mooring line for a vast range of frequencies, in order to demonstrate that our analytical expressions are accurate for all ranges of values of the parameters of the model. This is an important condition for the following sections, where real ocean measurements of a wide range of frequencies are incorporated in the computations. The results of such validation are shown in two figures, Figs. 3 and 4.

In particular, it is important to show that our results are accurate when compared to the numerical solution for different values of the parameter  $\gamma$ . This is the most important parameter to verify, since our analytical treatment is based on assumptions made over  $\gamma$ . By construction, our method should be very accurate when  $\gamma$  is considerably smaller than unit, and also when  $\gamma$  is considerably larger than unit; however, we expect less accuracy for moderate values of  $\gamma$ , on the order of unit. This is verified by the good agreement in the spatial profile of dynamic tension computed by a numerical solution and by our analytical solution, both for  $\gamma < 1$  [see Figs. 3(a) and 3(b)] as for  $\gamma > 1$  [see Figs. 3(e) and 3(f)].

In addition, Fig. 4 summarizes the good agreement between numerical and analytical computations of dynamic tension at the upper edge, for extensive simulations encompassing a wide range of frequencies and physical parameters. The accuracy of dynamic tension at the upper edge is important because it is the quantity that directly impacts in the prediction of stability of the floating structure, and also because most of the plots in figure. Figure 3 show that, despite moderate, the most significant deviation from exact and analytical tension in the spatial profile usually occurs close to the upper edge; thus, computation of the frequency spectrum at such position is adequate for the assessment of the largest error expected from our analytical results.

In summary, the analytical method is useful for all the ranges of the parameters employed in the model, which demonstrates the robustness of the analytical approach proposed in this work. This is particularly important to apply this solution in the study of ocean data, where it is required that the results work fine for the many spatial and time scales involved in the data. Such condition is related to the agreement between the analytical and the numerical solution for small and large values of the dimensionless frequency,  $\omega/\omega_c$ .

#### V. ANALYSIS OF *IN SITU* OCEAN DYNAMICS MEASUREMENTS: DISENTANGLING THE MULTI-SCALE CONTRIBUTIONS

The model used in this work has been adapted to account for waves and ocean current data measured and stored by the National



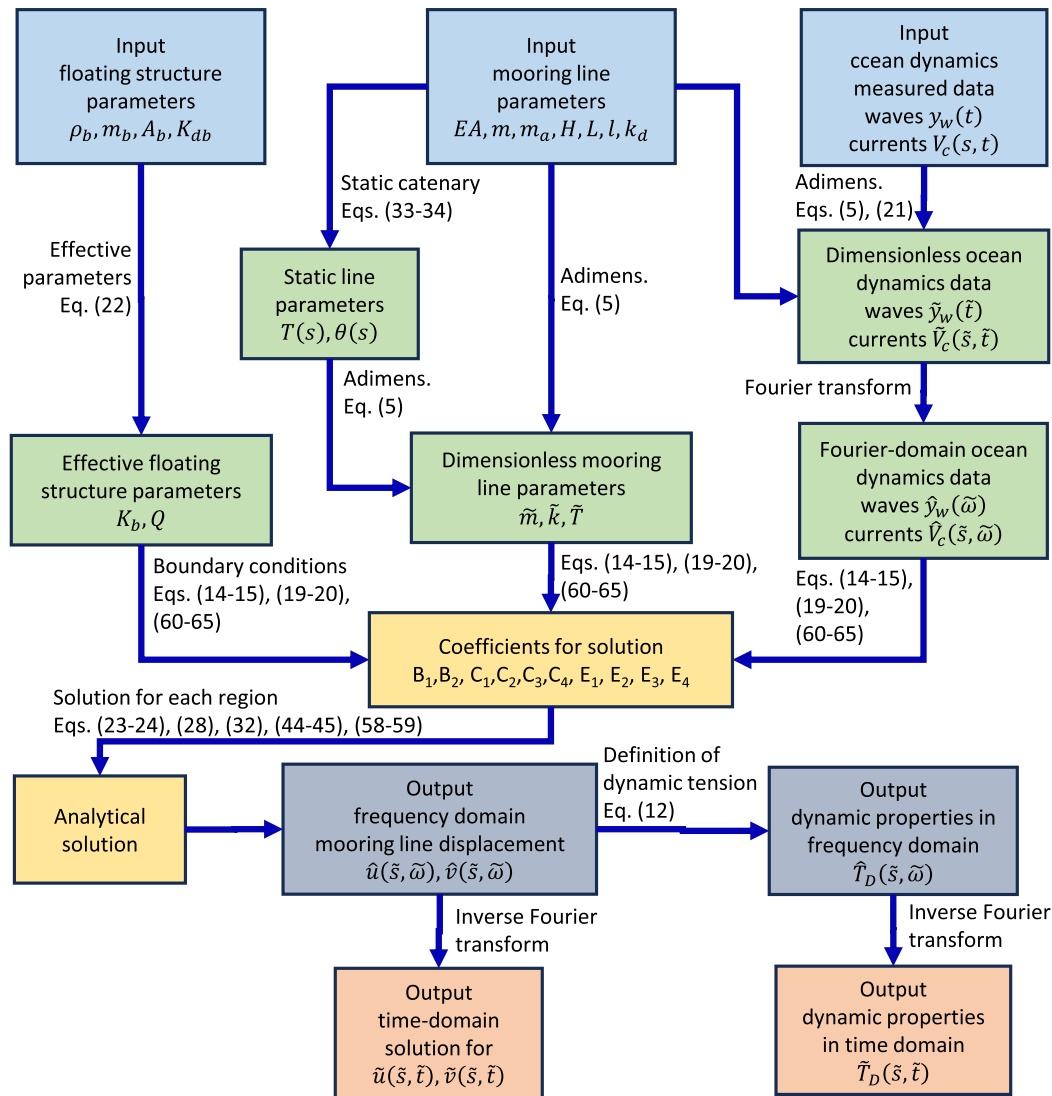


**FIG. 2.** Summary of the procedure to carry out the analytical solution by incorporation of all the physical parameters and measurements involved and the corresponding equations to carry out the treatment developed in this work.

Data Buoy System (Crout, 2022). Wave data used in this work correspond to the station 44005, while the ocean current data corresponds to the station 44032, located at Gulf of Maine, 78 NM East of Portsmouth, NH, USA. Records were processed, setting the begin of simulation time as  $t = 0$  on January 1st, 2022 at 0:00 h, local time (Data are processed with a technique that loses information of low frequency tidal waves).

In order to process and analyze these data, it is remarkable that dynamic tension, as defined in Eq. (3), can be decomposed in one term related to waves and another related to the ocean current. These terms are independent to one another, as exemplified below for the specific case of dynamic tension  $\hat{T}_D$  at the upper edge of mooring line, attached to the floating structure, which has the following form:

$$\hat{T}_D(\tilde{s} = 1, \tilde{\omega}) = R_w \hat{y}_w + \sum_{i=1}^2 R_{c,i} \int_0^1 \hat{V}_c(\tilde{s}', \tilde{\omega}) G_i(\tilde{s}', \tilde{\omega}) d\tilde{s}'. \quad (66)$$

This result is of relevance for processing and analysis of measurements of ocean waves and ocean currents separately, which is useful from a practical point of view. However, this is not in contradiction with the fact that ocean waves and currents are physically related, as has been extensively evidenced by several models on such currents/waves interaction (Longuet-Higgins and Stewart, 1962; Ardhuin *et al.*, 2008; and Umesh and Behera, 2020). In fact, any specific form of the interaction between ocean waves and currents can be tested by direct substitution of such relationship in the solution presented in this work. In consequence, the following study of ocean currents and waves will be carried out separately, providing useful results that can be employed and

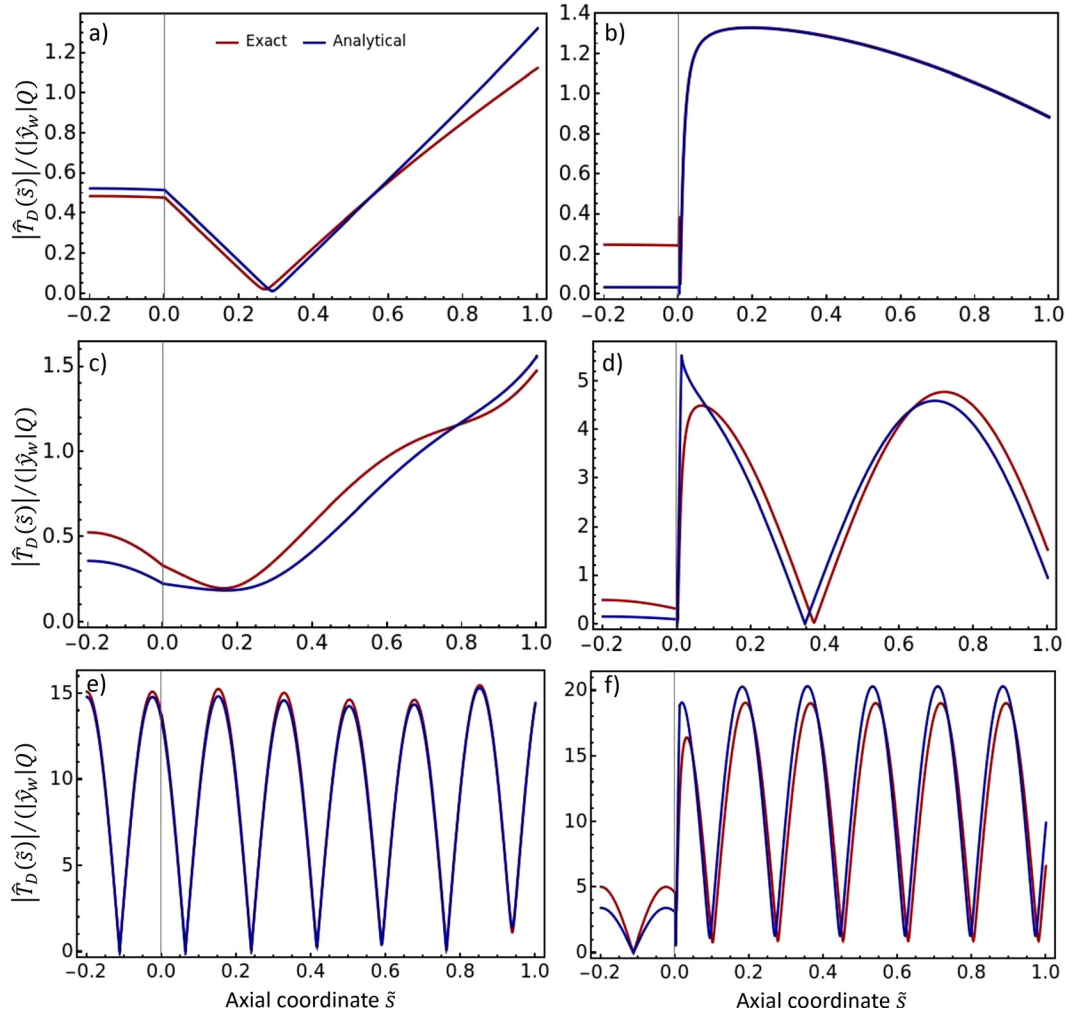


**FIG. 3.** Comparison of spatial profiles for the validation of analytical solution. Dynamic tension is computed for (a)  $\gamma = 0.5$  and  $\tilde{\omega} = 1$ ; (b)  $\gamma = 80$  and  $\tilde{\omega} = 1$ ; (c)  $\gamma = 0.5$  and  $\tilde{\omega} = 5$ ; (d)  $\gamma = 80$  and  $\tilde{\omega} = 5$ ; (e)  $\gamma = 0.5$  and  $\tilde{\omega} = 20$ ; and (f)  $\gamma = 80$  and  $\tilde{\omega} = 20$ . The following physical parameters were used in all the calculations:  $\tilde{k} = 10.0$ ,  $\tilde{m} = 0.8$ ,  $\tilde{l} = 0.2$ ,  $\varepsilon = 3.0$ ,  $K_b = 1.0 \times EA \sin \theta_0 / L$ ,  $K_{db} = 2.0 \times EA \sin \theta_0 / (\omega_c L)$ , and  $m_b = 5.0 \times EA \sin \theta_0 / (\omega_c^2 L)$ .

extrapolated to all kind of ocean measurements regardless of the specific form of the currents/waves interaction.

The impact of ocean currents in the dynamic tension of mooring lines not only depends on the magnitude of ocean flow velocity but also depends strongly on the coupling between the spatial modulation of ocean current and the elastic wave response contained in terms  $G_i(\tilde{s}', \tilde{\omega})$ , which turns out to be  $\sin(\sqrt{a \pm b\tilde{s}'})$  and  $\cos(\sqrt{a \pm b\tilde{s}'})$  in the region II, whereas it turns out to be  $I_0\sqrt{a\tilde{s}'}$  and  $K_0\sqrt{a\tilde{s}'}$  in the region III. In simple terms, this means that a certain modulation of flow velocity could enhance or suppress the impact of ocean currents beyond the magnitude of the average flow velocity, since both determine the magnitude of integrals in Eq. (66). This is depicted in Figs. 5(b) and 5(d), for four representative frequencies. A framework to account for the change of spatial profile in ocean current could be useful to extend the recent findings on complex ocean events observed recently by experimental and theoretical studies (Shrira and Almela, 2020).

For the study of wave dynamics, the analytical solution in this work provides a tool to analyze specific components of wave dynamics, both in time and in frequency domain. An inspection of Fig. 6(a) clearly exhibits that the dynamics of waves involves many characteristic frequencies, which are coupled harmonically with three different separations. The classification of the spectrum in regions is depicted in Fig. 6(a). Despite the location of each set of peaks is clear in frequency domain, their contribution to the net tension at each time is not evident. Moreover, it is of interest to explore whether they have an impact on the dynamics of the mooring line at all times or only at specific events.

In order to carry out such analysis, the linearity of the analytical solution is fundamental because it allows one to compute the mooring line tension for each of those regions independently, both in frequency and in time domain; then, the net dynamic tension in time domain will be the sum of all the contributions. The components of dynamic tension are depicted in Figs. 6(a) and 6(b). It is noticed that none of

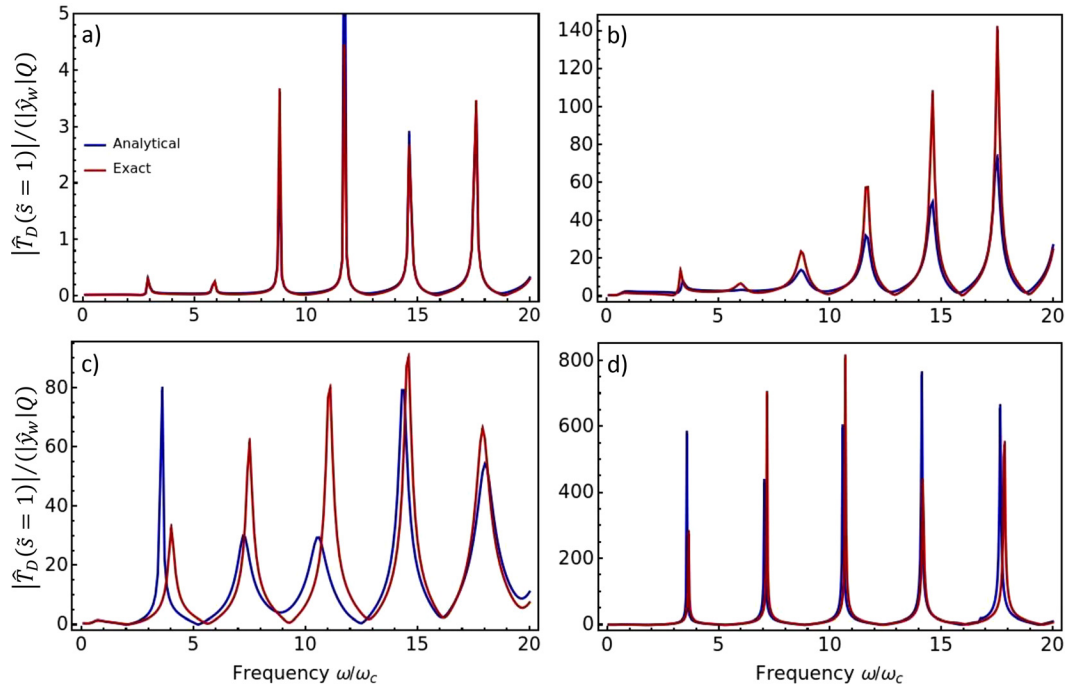


**FIG. 4.** Validation of analytical solution under difficult conditions of simulation. Global comparison of tension at the attachment with the platform for many frequencies of excitation, considering (a)  $\gamma = 0.01$ , (b)  $\gamma = 1$ , (c)  $\gamma = 10$ , and (d)  $\gamma = 100$ . The following physical parameters were used in all the calculations:  $k = 10.0$ ,  $\bar{m} = 0.8$ ,  $\bar{l} = 0.2$ ,  $\varepsilon = 3.0$ ,  $K_b = 1.0 \times EA \sin \theta_0 / L$ ,  $K_{db} = 2.0 \times EA \sin \theta_0 / (\omega_c L)$ , and  $m_b = 5.0 \times EA \sin \theta_0 / (\omega_c^2 L)$ .

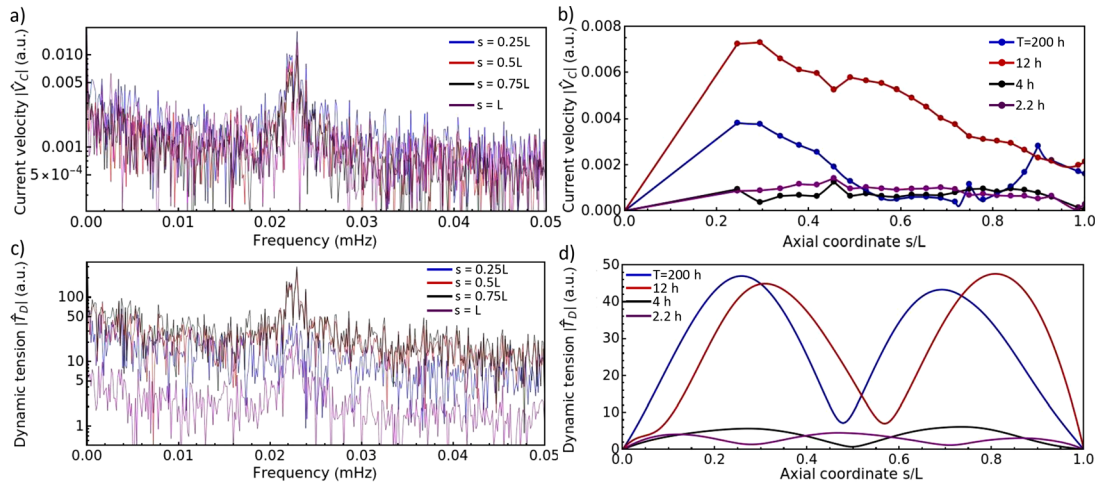


**FIG. 5.** Influence of frequency and spatial dependence of ocean current flow velocity in the mooring line. Left-side plots correspond to the frequency spectrum of (a) current velocity and (c) dynamic tension, each curve corresponds to a specific position within the mooring line. Right-side plots correspond to the spatial profiles of (b) current velocity and (d) dynamic tension, each curve corresponds to a specific frequency. The following physical parameters were used:  $\bar{m} = 1.0$ ,  $V_{c0} = 2.0$  m/s,  $diam = 0.109$  m,  $m = 49.0$  kg/m,  $h = 100.0$  m,  $L = 150$  m,  $l = 15$  m,  $EA = 5.37 \times 10^8$  N,  $\rho_b = 800$  kg/m<sup>3</sup>,  $R_b = 10$  m, and  $m_b = 2.5 \times 10^5$  kg.

these components is negligible in net dynamic tension; moreover, each component has different roles in the global response at specific times and events. The low-frequency region of ocean waves spectrum (blue zone) has a very homogeneous contribution to the dynamic tension in

time domain in the time frame plotted [see Fig. 6(b)]. The middle-frequency region (green zone) is the main contribution for the high-amplitude events in lapses 120–135 s and 165–178 s, while the high-frequency region (black zone) is the main contribution to

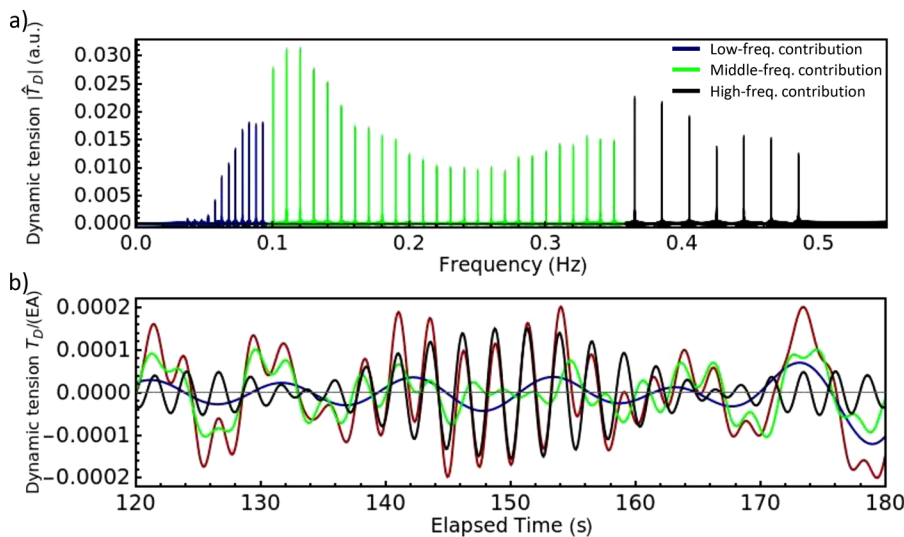


**FIG. 6.** Analysis of the contributions to the dynamic tension, caused by each region of the Fourier spectrum of wave dynamics. (a) Definition of each region in frequency domain, blue for low-frequency region, green for middle-frequency region, and black for high-frequency region. (b) Contribution of each subset of peaks to the tension in time domain (plotted in blue, green, and black), along with the net dynamic tension (red line). The physical parameters are identical to the ones employed in Fig. 5.

dynamic tension in time lapse 140–155 s. From the aforementioned analysis, it is clear that the low-frequency peaks contribute significantly to the net tension at all times; in contrast, certain anomalous events are dominated by the middle-frequency peaks, while other anomalous events are dominated by the high-frequency peaks. In this manner, our analytical results could provide a framework to combine frequency- and time-domain studies of anomalous ocean events (Janssen and Janssen, 2019).

The analysis presented in this work can be applied directly to most of the data acquired from basic buoys that measure ocean waves dynamics, since the average change of sea level is the most fundamental feature recorded by such devices. In such a regard, this is a tool of general applicability. Moreover, it can be extended to account for specialized buoys that also record vector information about the time-dependent directionality of ocean waves. The results presented here could be extended for that case, with two considerations. First, the spatial dependence of sea level produces a secondary lateral oscillation of the floating structure, that is modeled by a torque balance incorporated as a second equation in addition to the force balance in Eq. (16); nonetheless, the torque balance is complementary with the force balance already presented, so the spatially averaged vertical motion of the mooring line would be consistent with the results presented in this work. Second, the lateral oscillation of the floating structure produces a complex three-dimensional mooring line motion that is not considered in this work; however, the component in the direction of the static deflection of mooring line plays the dominant role in the global mooring line dynamics. In summary, the results presented in this work are a departing point that provides the dominant and most important features of mooring line dynamics so the incorporation of directionality of ocean waves will expand and complement these results.

## VI. COMPUTATIONAL IMPLICATIONS IN PROCESSING OF OCEAN CURRENTS DATA: ROLE OF DATA INTERPOLATION

One of the major difficulties in the incorporation of real ocean current measurements into simulation of mooring lines is related to

their low resolution. As an example, in the cases studied in this work, the resolution is on the order of 10 m. For this reason, an appropriate strategy of data interpolation is fundamental in simulations. In all the numerical methods of solution, the discretization of spatial coordinate into domains or regions causes mathematical artifacts that interfere with the complex spatial profile of ocean current velocity, and the role of flow velocity interpolation on simulations is not evident.

In contrast with the aforementioned limitations, the analytical solution in this work exhibits clearly and concisely the role of ocean current interpolation in the utter dynamics of mooring lines. This is summarized in Fig. 7.

From a mathematical point of view, it is clear by inspection of the analytical solution that the incorporation of ocean current data requires to compute integrals of a complex kernel multiplied by the ocean current velocity profile. Therefore, the condition to guaranty that no artifact is produced during such interpolation of ocean current data only requires to guaranty that the integrals done in Eqs. (44), (45), (58), and (59) are convergent, which is a condition easily achievable as far as the interpolation function used is also convergent. However, more importantly, the convergence of such integral is considerably less challenging than the convergence of any numerical method of solution of differential equations. This property demonstrates the robustness of the analytical treatment carried out in this work.

From a computational point of view, Fig. 7 shows that a small change in the interpolation technique used in current velocity profiles has a considerable impact on the simulated dynamic tension profile. In particular, four kinds of interpolation techniques are exemplified, two classical methods that preserve the input points (namely, linear and quadratic interpolation) and two methods widely used in data science to reduce small range variation of data, in an attempt to focus on the main qualitative trends of curves. Such techniques are the B-Spline function and the Bézier function. It is clear that the particular choice of an interpolation technique leads to different values of dynamic tension along the mooring line, despite the overall profile is preserved in all cases.

Our results are free from artifacts caused by discretization; in consequence, we expect that such a strong dependence on the choice of an



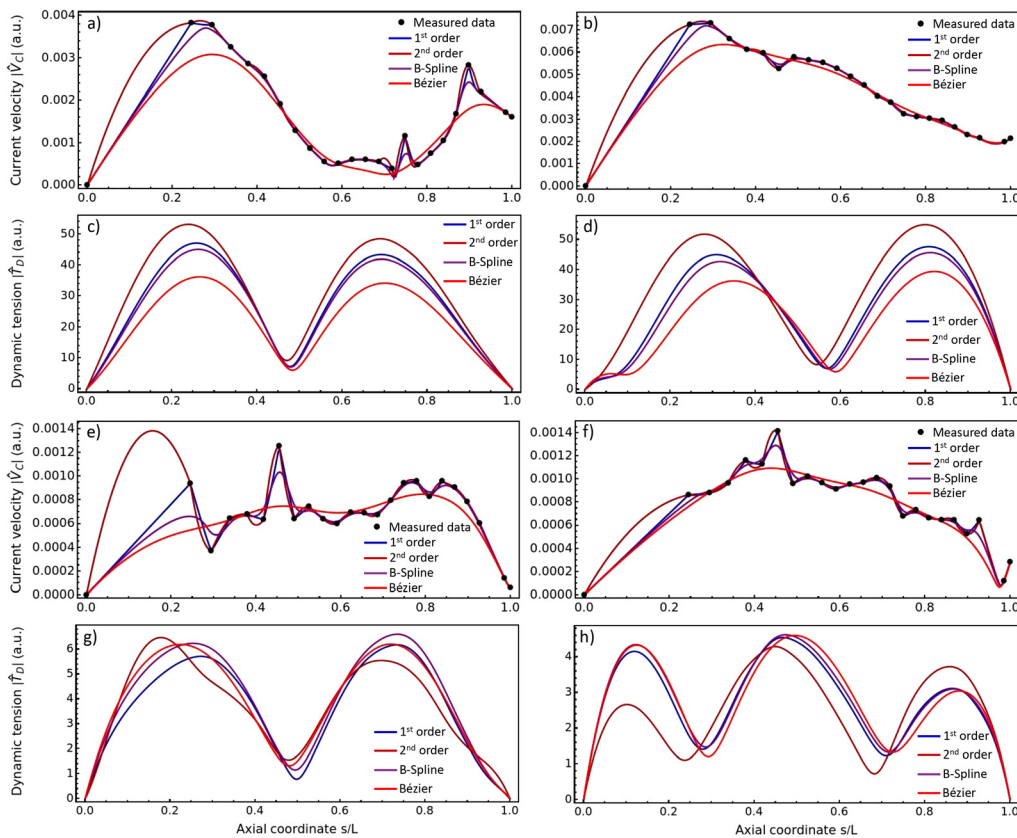


**FIG. 7.** Influence of interpolation technique for processing of ocean current data. The spatial profile for four representative frequencies are presented, which correspond to a period of 200 h (a) and (c), 12 h (b) and (d) that correspond to the maxima of ocean current spectrum, 4 h (e) and (g), and 2.2 h (f) and (h). For each frequency, the spatial profile of both the flow velocity and dynamic tension is plotted. The physical parameters are identical to the ones employed in Fig. 5.

interpolation technique will remain or even increase when more sophisticated models are employed in the future. This constitutes a current challenge to be faced by all the simulations that attempt to incorporate real measurements of current ocean profiles in future simulations of mooring lines under realistic environmental conditions. Another challenge faced by numerical methods refers to computations involving large magnitudes of the physical parameters or for ocean waves and currents of large amplitude. Typically, numerical methods lead to instability when dealing with large amplitude excitations; this concern is completely absent in our analytical results. The only concern when dealing with ocean waves and currents of large amplitude is to verify that the small amplitude vibration is still valid, which is a limitation of the model employed in this work.

## VII. CONCLUSION

The analytical results presented here provide a robust framework for the computation of mooring system dynamics under realistic conditions of arbitrary complexity. By the incorporation of ocean waves and ocean currents data that spread a wide range of characteristic frequencies and wavelengths, we have demonstrated that our analytical results are capable to simulate all this range of variables and conditions with very good accuracy and without concerns on the stability or computational expense of simulations.

With such tools, we have described the qualitative role of ocean currents and waves in the dynamic behavior of mooring systems. In particular, the importance of the coupling between frequency and spatial modulation of ocean currents is clearly exposed both in the analytical expressions and in the computations presented. In addition, we have shown the advantages of this approach to analyze every feature encountered in ocean waves and currents, by combining time- and frequency-domain computations. This is particularly important for identification and classification of oceanic events in terms of their impact on the behavior of floating structures. Clearly, a comprehensive effort to carry out such classification would require several transversal studies of oceanic data, based upon the results of this work.

Our results rely on the assumptions of the model employed, which considers an initial equilibrium configuration that can be arbitrarily deformed; then, the dynamics is studied under the assumption that the amplitude of mooring line motion only deviates moderately from equilibrium. In practical terms, our results will provide quantitative and qualitative useful prediction of the dynamics of mooring systems even if the initial catenary configuration exhibits a large deformation, as far as the vibration is of low to moderate magnitude; however, the model will present a significant error for mooring line vibration of large magnitude, and our analytical results inherit the same limitations. Furthermore, other studies on the non-modal



dynamics of mooring lines affected by vortex-induced motion are relevant and complementary to this analytical study.

Despite these limitations, qualitative trends such as the arising of resonances and the magnitude of dynamic tension will remain in good agreement with experiments at conditions of small amplitude oscillations. Moreover, our analytical expressions produce simulations where realistic environmental conditions can be implemented and analyzed with confidence, and they can be contrasted against more sophisticated simulations for the detection of spurious numerical artifacts. Those artifacts can be found in sophisticated numerical simulations under challenging or extreme conditions, but they are intrinsically absent in our analytical framework. Additionally, our insights could facilitate subsequent analysis and reduce the computational expense of more sophisticated simulations, by focusing on specific features unveiled with our analytical tools. In all cases, our results have the perspective to be used as a validation and departing point for more sophisticated simulations.

The robustness of our analytical results is of special interest for future applications toward the optimization of operation and design parameters of offshore floating structures. Optimization of simulated complex systems is a current task in all areas of science and engineering, given its computational cost; our results are useful in that regard because they allow us to compute derivatives of any target property in terms of all the physical parameters presented in the simulations, with a minimal computational time and without further refining and verification, as occurs when computing numerical derivatives by discretization approaches. This reduces the computational time of each optimization step and opens a wider gamma of faster and more robust methods of solution that are not typically available when dealing with complex systems (Dinh *et al.*, 2016; Audet *et al.*, 2017; and Larson *et al.*, 2019). Analytical results combined with optimization techniques offer a panorama for better tools for improved design and performance of floating structures.

An improved description and understanding of ocean phenomena, in terms of their impact in marine structures, could be useful for the assessment of extreme environmental conditions. Specially, the results in this work exemplify the role of ocean current modulation and the multi-scale nature of ocean waves, as observed in *in situ* measurements. This is a present and future challenge for the assessment of marine structures under the environmental conditions produced by climate change.

## ACKNOWLEDGMENTS

This research work was supported by (1) the Research Grants Council (RGC) of the Hong Kong University Grants Committee (UGC) (Project No. C5002-22Y) and (2) the Hong Kong Polytechnic University (Project No. 4-ZZNF).

## AUTHOR DECLARATIONS

### Conflict of Interest

The authors have no conflicts to disclose.

## Author Contributions

**Ulises Torres-Herrera:** Conceptualization (equal); Data curation (equal); Formal analysis (equal); Investigation (equal); Methodology

(equal); Software (equal); Validation (equal); Visualization (equal); Writing – original draft (equal); Writing – review & editing (equal). **Alireza Keramat:** Conceptualization (equal); Investigation (equal); Project administration (supporting); Resources (supporting); Supervision (supporting); Validation (supporting); Writing – original draft (supporting). **Huan-Feng Duan:** Conceptualization (equal); Funding acquisition (equal); Investigation (equal); Project administration (equal); Resources (equal); Supervision (equal).

## DATA AVAILABILITY

The data that support the findings of this study are available from the corresponding author upon reasonable request.

## NOMENCLATURE

### List of symbols and notation

$A$	cross-sectional area of mooring line, in $\text{m}^2$
$A_b$	cross-sectional area of cylindrical floating structure, in $\text{m}^2$
$a$	parameter related to wave modulation, dimensionless
$b$	parameter related to wave modulation, dimensionless
$B_1$	integration constant for solution of region I, dimensionless
$B_2$	integration constant for solution of region I, dimensionless
$C_1$	integration constant for solution of region II, dimensionless
$C_2$	integration constant for solution of region II, dimensionless
$C_3$	integration constant for solution of region II, dimensionless
$C_4$	integration constant for solution of region II, dimensionless
$E$	Young's modulus, in Pa
$E_1$	integration constant for solution of region III, dimensionless
$E_2$	integration constant for solution of region III, dimensionless
$E_3$	integration constant for solution of region III, dimensionless
$E_4$	integration constant for solution of region III, dimensionless
$g$	gravitational acceleration, in $\text{m} \cdot \text{s}^{-2}$
$H$	horizontal component of static tension of mooring line, in N
$I_0$	modified zeroth-order Bessel function of the first kind, dimensionless
$I_1$	modified first-order Bessel function of the first kind, dimensionless
$K_0$	modified zeroth-order Bessel function of the second kind, dimensionless
$K_1$	modified first-order Bessel function of the second kind, dimensionless
$K_b$	constant of buoyant force acting on floating structure, in $\text{N} \cdot \text{m}^{-1}$
$K_{ab}$	drag coefficient of floating structure, in $\text{N} \cdot \text{s} \cdot \text{m}^{-1}$
$\tilde{k}$	dimensionless drag coefficient of mooring line
$k_d$	drag coefficient of mooring line, in $\text{N} \cdot \text{s} \cdot \text{m}^{-2}$
$L$	length of detached portion of mooring line, in m
$l$	length of mooring line portion attached to seabed, in m
$\underline{M}$	characteristic matrix associated to solution in region I, dimensionless
$m$	mass-per-unit-length of mooring line, in $\text{kg} \cdot \text{m}^{-1}$
$m_a$	added mass-per-unit-length of mooring line, in $\text{kg} \cdot \text{m}^{-1}$
$m_b$	mass of cylindrical floating structure, in kg
$\tilde{m}$	dimensionless mass-per-unit-length of mooring line

$Q$	parameter related to wave/floating structure interaction, dimensionless
$R_w$	effective amplitude of dynamic tension at top of mooring line caused by waves, dimensionless
$R_{c,i}$	effective amplitude of dynamic tension at top of mooring line caused by interaction of ocean current with $i$ -th modulation of mooring line, dimensionless
$s$	spatial coordinate tangential to the mooring line at equilibrium, in m
$\tilde{s}$	dimensionless spatial coordinate tangential to the mooring line at equilibrium
$s_{th}$	threshold value of axial coordinate for transition between region II and region III, dimensionless
$\tilde{s}'$	integration variable associated to dimensionless spatial coordinate, dimensionless
$t$	time, in s
$\tilde{t}$	dimensionless time
$T$	static tension along the mooring line in equilibrium, in N
$\tilde{T}$	dimensionless static tension along the mooring line
$T_d$	dynamic tension along the mooring line, in N
$\tilde{T}_d$	dimensionless dynamic tension along the mooring line
$\hat{T}_d$	Fourier transform in time of dimensionless dynamic tension, dimensionless
$u$	axial mooring line displacement, in m
$\tilde{u}$	dimensionless axial mooring line displacement
$\hat{u}$	Fourier transform in time of dimensionless axial mooring line displacement, dimensionless
$\tilde{u}_I$	axial mooring line displacement at region I, dimensionless
$\tilde{u}_{II}$	axial mooring line displacement at region II, dimensionless
$\tilde{u}_{III}$	axial mooring line displacement at region III, dimensionless
$U_w$	dimensionless amplitude of mono-modal wave, dimensionless
$v$	transversal mooring line displacement, in m
$\tilde{v}$	dimensionless transversal mooring line displacement
$\hat{v}$	Fourier transform in time of dimensionless transversal mooring line displacement, dimensionless
$\tilde{v}_I$	transversal mooring line displacement at region I, dimensionless
$\tilde{v}_{II}$	transversal mooring line displacement at region II, dimensionless
$\tilde{v}_{III}$	transversal mooring line displacement at region III, dimensionless
$V_c$	ocean current flow velocity, in $\text{m} \cdot \text{s}^{-1}$
$\tilde{V}_c$	dimensionless ocean current flow velocity, dimensionless
$\hat{V}_c$	Fourier transform in time of dimensionless ocean current flow velocity, dimensionless
$y_b$	vertical displacement of floating structure, in m
$y_w$	vertical displacement of ocean waves, in m
$\hat{y}_w$	Fourier transform in time of dimensionless vertical displacement of ocean waves, dimensionless
$\alpha$	parameter related to wave modulation, dimensionless
$\gamma$	effective length of mooring line, dimensionless
$\varepsilon$	dimensionless static tension, dimensionless
$\theta$	static contact angle along the mooring line in equilibrium, in rad
$\theta_{top}$	static contact angle at the attachment point with the floating structure, in rad

$\lambda$	eigenvalue, dimensionless
$\rho_w$	density of water, in $\text{kg} \cdot \text{m}^{-3}$
$\rho_w$	density of cylindrical floating structure, in $\text{kg} \cdot \text{m}^{-3}$
$\varphi$	dynamic angle, in rad
$\omega_c$	characteristic frequency, in $\text{rad} \cdot \text{s}^{-1}$
$\tilde{\omega}$	dimensionless frequency

## REFERENCES

- Ali, M. O. A., Ja'e, I. A., and Hwa, M. G. Z., "Effects of water depth, mooring line diameter and hydrodynamic coefficients on the behaviour of deepwater FPSOs," *Ain Shams Eng. J.* **11**, 727–739 (2020).
- Aranha, J. A. P. and Pinto, M. O., "Dynamic tension in risers and mooring lines: An algebraic approximation for harmonic excitation," *Appl. Ocean Res.* **23**, 63–81 (2001).
- Aranha, J., Pesce, C., Martins, C., and Andrade, B., "Mechanics of submerged cables: Asymptotic solution and dynamic tension," in *International Ocean and Polar Engineering Conference, Volume All Days of International Ocean and Polar Engineering Conference* (ISOPE, 1993).
- Ardhuin, F., Rasche, N., and Belibassakis, K. A., "Explicit wave-averaged primitive equations using a generalized Lagrangian mean," *Ocean Modell.* **20**, 35–60 (2008).
- Audet, C., Hare, W., Audet, C., and Hare, W., *Introduction: Tools and Challenges in Derivative-Free and Blackbox Optimization* (Springer, 2017).
- Azcona, J., Munduate, X., González, L., and Nygaard, T. A., "Experimental validation of a dynamic mooring lines code with tension and motion measurements of a submerged chain," *Ocean Eng.* **129**, 415–427 (2017).
- Barrera, C., Guanche, R., and Losada, I. J., "Experimental modelling of mooring systems for floating marine energy concepts," *Mar. Struct.* **63**, 153–180 (2019).
- Bernitsas, M. M. and Garza-Rios, L. O., "Turret mooring design based on analytical expressions of catastrophes of slow-motion dynamics," *J. Offshore Mech. Arct. Eng.* **120**, 154–164 (1998).
- Cheng, H., Li, L., Ong, M. C., Aarsaether, K. G., and Sim, J., "Effects of mooring line breakage on dynamic responses of grid moored fish farms under pure current conditions," *Ocean Eng.* **237**, 109638 (2021).
- Crout R. (2022). "Documentation for National Data Buoy Center (NDBC) Tropical Atmosphere Ocean (TAO) array moored buoy data archived at NCEI (NCEI accession 0088104)," NOAA national centers for environmental information. <https://www.ncei.noaa.gov/archive/accession/0088104>.
- de Langre, E., Paidoussis, M., Doaré, O., and Modarres-Sadeghi, Y., "Flutter of long flexible cylinders in axial flow," *J. Fluid Mech.* **571**, 371–389 (2007).
- Desiré, P., Rodríguez-Luis, A., and Guanche, R., "Simulation of mooring lines in complex bathymetries using a finite element method," *Ocean Eng.* **272**, 113827 (2023).
- Dinh, V. B., Delinchant, B., and Wurtz, F., "The importance of derivatives for simultaneous optimization of sizing and operation strategies: Application to buildings and HVAC systems," in *Building Simulation and Optimization (BSO2016)* (IBPSA, Newcastle, United Kingdom, 2016), pp. 1–7.
- Du, J., Wang, H., Wang, S., Song, X., Wang, J., and Chang, A., "Fatigue damage assessment of mooring lines under the effect of wave climate change and marine corrosion," *Ocean Eng.* **206**, 107303 (2020).
- Fu, S., Jin, Y., Zheng, Y., and Chamorro, L. P., "Wake and power fluctuations of a model wind turbine subjected to pitch and roll oscillations," *Appl. Energy* **253**, 113605 (2019).
- Ghafari, H. and Dardel, M., "Parametric study of catenary mooring system on the dynamic response of the semi-submersible platform," *Ocean Eng.* **153**, 319–332 (2018).
- Governo, A., Henriques, J., and Gato, L., "Modelling mooring line snap loads using a high-order finite-volume approach," *Ocean Eng.* **275**, 113803 (2023).
- Grare, L., Peirson, W. L., Branger, H., Walker, J. W., Giovanangeli, J.-P., and Makin, V., "Growth and dissipation of wind-forced, deep-water waves," *J. Fluid Mech.* **722**, 5–50 (2013).
- Hong, K.-S. and Shah, U. H., "Vortex-induced vibrations and control of marine risers: A review," *Ocean Eng.* **152**, 300–315 (2018).
- Huguet, J.-R., Brenon, I., and Coulombier, T., "Influence of floating structures on tide-and wind-driven hydrodynamics of a highly populated marina," *J. Waterway, Port, Coastal, Ocean Eng.* **146**, 05019004 (2020).

- Irvine, H. M. and Caughey, T. K., "The linear theory of free vibrations of a suspended cable," *Proc. Math. Phys. Eng. Sci.* **341**, 299–315 (1974).
- Ja'e, I. A., Ali, M. O. A., Yenduri, A., Nizamani, Z., and Nakayama, A., "Optimisation of mooring line parameters for offshore floating structures: A review paper," *Ocean Eng.* **247**, 110644 (2022).
- Janssen, P. A. E. M. and Janssen, A. J. E. M., "Asymptotics for the long-time evolution of kurtosis of narrow-band ocean waves," *J. Fluid Mech.* **859**, 790–818 (2019).
- Kuehl, J. J. and Sheremet, V. A., "Two-layer gap-leaping oceanic boundary currents: Experimental investigation," *J. Fluid Mech.* **740**, 97–113 (2014).
- Larson, J., Menickelly, M., and Wild, S. M., "Derivative-free optimization methods," *Acta Numer.* **28**, 287–404 (2019).
- Longuet-Higgins, M. S. and Stewart, R., "Radiation stress and mass transport in gravity waves, with application to 'surf beats'," *J. Fluid Mech.* **13**, 481–504 (1962).
- Ma, K.-T., Luo, Y., Kwan, C.-T. T., and Wu, Y., *Mooring System Engineering for Offshore Structures* (Gulf Professional Publishing, 2019).
- Matha, D., Schlipf, M., Pereira, R., and Jonkman, J., "Challenges in simulation of aerodynamics, hydrodynamics, and mooring-line dynamics of floating offshore wind turbines," in *ISOPE International Ocean and Polar Engineering Conference* (ISOPE, 2011).
- Ramadan, M. A., Raslan, K. R., El Danaf, T. S., and Salam, M. A. E., "Solving systems of high-order ordinary differential equations with variable coefficients by exponential Chebyshev collocation method," *J. Mod. Methods Numer. Math.* **8**, 40–51 (2017).
- Ruzzo, C., Muggiasca, S., Malara, G., Taruffi, F., Belloli, M., Collu, M., Li, L., Brizzi, G., and Arena, F., "Scaling strategies for multi-purpose floating structures physical modeling: State of art and new perspectives," *Appl. Ocean Res.* **108**, 102487 (2021).
- Shrira, V. I. and Almelah, R. B., "Upper-ocean Ekman current dynamics: A new perspective," *J. Fluid Mech.* **887**, A24 (2020).
- Shun-Han Yang, E. J., Ringsberg, J. W., and Hu, Z., "Experimental and numerical investigation of a taut-moored wave energy converter: A validation of simulated mooring line forces," *Ships Offshore Struct.* **15**, S55–S69 (2020).
- Sinsabvarodom, C., Leira, B. J., Chai, W., and Naess, A., "Short-term extreme mooring loads prediction and fatigue damage evaluation for station-keeping trials in ice," *Ocean Eng.* **242**, 109930 (2021).
- Subbulakshmi, A., Verma, M., Keerthana, M., Sasmal, S., Harikrishna, P., and Kapuria, S., "Recent advances in experimental and numerical methods for dynamic analysis of floating offshore wind turbines—An integrated review," *Renewable Sustainable Energy Rev.* **164**, 112525 (2022).
- Tang, H.-J., Yao, H.-C., and Yang, R.-Y., "Experimental and numerical studies on successive failures of two mooring lines of a net cage subjected to currents," *Ocean Eng.* **266**, 113243 (2022).
- Torres-Herrera, U. and Corvera Poiré, E., "A continuum model to study fluid dynamics within oscillating elastic nanotubes," *J. Fluid Mech.* **916**, A16 (2021).
- Triantafyllou, M. S., "Preliminary design of mooring systems," *J. Ship Res.* **26**, 25–35 (1982).
- Umesh, P. and Behera, M. R., "Performance evaluation of input-dissipation parameterizations in WAVEWATCH III and comparison of wave hindcast with nested WAVEWATCH III-SWAN in the Indian seas," *Ocean Eng.* **202**, 106959 (2020).
- Yang, Y., Bashir, M., Li, C., and Wang, J., "Investigation on mooring breakage effects of a 5 mw barge-type floating offshore wind turbine using f2a," *Ocean Eng.* **233**, 108887 (2021).
- Zurigat, M., Momani, S., Odibat, Z., and Alawneh, A., "The homotopy analysis method for handling systems of fractional differential equations," *Appl. Math. Model.* **34**, 24–35 (2010).